

BS18

Using Ghost Reflections Rather than Removing Them

G. Blacquiere* (Delft University of Technology) & A.J. Berkhout (Delft University of Technology)

SUMMARY

In marine acquisition both a direct wavefield and a ghost wavefield are produced as well as recorded. Hence, the seismic data can be considered to be a natural blend of four wavefields related to the real sources, ghost sources, real detectors and ghost detectors respectively. We consider deghosting to be deblending ('echo-deblending'), leading to a non-causal, full-wavefield algorithm, characterized by utilizing the ghost. Therefore, echo-deblending is different from prediction-error solutions that aim at removing the ghost.

Echo-deblending is independent of the subsurface complexity; only what happens at and near the surface is relevant. Depending on the sea state, the reflection coefficient is frequency dependent. Moreover, the water velocity varies due to variations in temperature, salinity and pressure. We propose to measure such parameters and/or estimate them from the data.

The output of our method consists of four ghost-free records: one due to real sources at the actual location below the water level (+zs), one due to ghost source at the mirrored location above the water level (-zs), both being recorded by real detectors at (+zd) and by ghost detectors at (-zd). Optionally, these four records are transformed to one record at a common source-receiver datum (z0).

Introduction

In marine acquisition, the source and detector ghosts cause the well-known angle-dependent notches in the spectrum. In addition, the low frequencies are severely attenuated. In this paper we do not focus on hardware solutions such as multi-level source arrays or multi-component streamer technology. Instead, we focus on deghosting as a preprocessing step in the case of standard seismic acquisition. Many methods for deghosting have been proposed. E.g., Soubaras (2010) carries out joint deconvolution to a direct and a mirror migration result; Wang and Peng (2012) introduce a bootstrap method based on modelled mirror data; Amundsen et al. (2013) apply a frequency-domain spatial deconvolution; Beasley et al. (2013) and Robertsson et al. (2014) exploit causality: upcoming waves arrive earlier than the corresponding downgoing 'ghost' waves; Ferber and Beasley (2014) shift the ghost events out of the time window. Some examples specifically focussing at the source side are Mayhan and Weglein (2013) and Amundsen and Zhou (2013).

Here, we treat deghosting as deblending ('echo-deblending'), leading to a non-causal, full-wavefield algorithm where the ghost reflections are utilized (Berkhout and Blacqui re, 2014). Therefore, it is principally different from a prediction-error solution that aims at removing the ghost reflections. Echo-deblending is independent of the complexity of the subsurface; only the ghost-model, i.e., what happens at and near the surface, is relevant: the sea surface reflectivity (Orji et al., 2013) and the propagation velocity in the water (Leroy et al., 2008).

Method and Theory

In this section we discuss the case of source deghosting. In marine acquisition, the sources are towed at some depth $+z_s$ below the surface z_0 . This tow depth may be spatially variable, i.e., $z_s = z_s(x,y)$. Due to the strong water surface reflectivity two source wavefields of comparable strength are generated: the first is travelling down, the second is going up, getting reflected at the water surface and then travelling down (Figure 1a). The latter generates the ghost response. An attractive way to model this is to consider a situation without air and to add mirrored 'ghost' sources above the surface to 'real' sources below the surface (Figure 1b). This represents a *blending* process, the blending being vertical and natural:

$$\mathbf{P}^-(z_0; \pm z_s) = \mathbf{P}^-(z_0; z_0) [\mathbf{F}^-(z_0, +z_s) - \mathbf{R}\mathbf{W}^+(z_0, -z_s)]. \quad (1)$$

Here $\mathbf{P}(z_0; \pm z_s)$ is the data matrix. Every row represents one frequency component of a common detector gather, the detector depth being z_0 and every column represents one shot record, the source depth being $\pm z_s(x,y)$. The symbol \pm indicates the presence of both real sources (at $+z_s$) and ghost sources (at $-z_s$). \mathbf{F} and \mathbf{W} represent reverse and forward extrapolation respectively, their superscripts $-$ and $+$ indicating the upward and downward direction respectively, and $-\mathbf{R}$ represents the angle- and frequency dependent reflectivity of the surface. The minus sign emphasizes the pressure polarity reversal involved. The fact that \mathbf{F} and \mathbf{W} are applied at the right-hand side of \mathbf{P} means that common receiver gathers are extrapolated. For details about the matrix notation see Berkhout (1982).

Our closed-loop, iterative echo-deblending method is making use of *both* the real sources and the ghost sources. We start by computing two estimates for the response due to sources at the surface, one

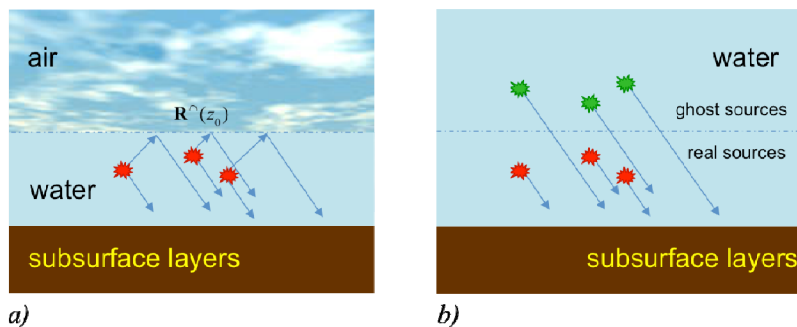


Figure 1 The source-related ghost response in marine data is caused by the strong surface reflectivity (a). It can be represented by the response of so-called ghost sources (b).

related to the real sources and one related to the ghost sources, respectively:

$$\langle \mathbf{P}^-(z_0; z_0) \rangle_{real} = \langle \mathbf{P}^-(z_0; +z_s) \rangle \mathbf{W}^+(+z_s, z_0) \quad (2)$$

$$\langle \mathbf{P}^-(z_0; z_0) \rangle_{ghost} = -\langle \mathbf{P}^-(z_0; -z_s) \rangle \mathbf{F}^-(-z_s, z_0) \mathbf{R}^{-1}. \quad (3)$$

Brackets $\langle \rangle$ and $\langle \rangle$ indicate an estimate. In the first iteration the estimates at $+z_s$ and $-z_s$ are both given by the measured data: $\langle \mathbf{P}^-(z_0; -z_s) \rangle = \langle \mathbf{P}^-(z_0; +z_s) \rangle = \mathbf{P}^-(z_0; \pm z_s)$. (4)

In equation (2) the real sources are moved up to the surface and in equation (3) the ghost sources are moved down to the surface while the effect of the surface reflectivity has been removed (Figures 2, 3). If we average the responses of equations (2) and (3) and substitute equation (1) in the result, we get:

$$\langle \mathbf{P}^-(z_0; z_0) \rangle = \mathbf{P}^-(z_0; z_0) [\mathbf{F}^- - \mathbf{R}\mathbf{W}^+] [\mathbf{W}^+ - \mathbf{F}^- \mathbf{R}^{-1}], \text{ or,} \quad (5)$$

$$\langle \mathbf{P}^-(z_0; z_0) \rangle = \mathbf{P}^-(z_0; z_0) \left[\mathbf{I} - \frac{1}{2} \mathbf{F}^- \mathbf{F}^- \mathbf{R}^{-1} - \frac{1}{2} \mathbf{R}\mathbf{W}^+ \mathbf{W}^+ \right]. \quad (6)$$

Here we simplified the notation. Expression (6) shows that this estimate, which has been obtained by utilizing the responses of both the real sources and the ghost sources, indeed contains the desired response. However, in addition it contains two undesired responses as well (Figure 2c). Fortunately, their amplitudes are approximately half. This means that a nonlinear filtering step, such as time-domain thresholding, can be used to suppress the undesired responses while preserving part of the desired responses (Figure 2d). Once extrapolated to $+z_s$ and $-z_s$ respectively, this nonlinear-filter result can be adaptively subtracted from the measured data to get new, conservative estimates corresponding to the real sources at $-z_s$ and the ghost sources at $+z_s$ respectively:

$$\langle \mathbf{P}^-(z_0; +z_s) \rangle = \mathbf{P}^-(z_0; \pm z_s) - \mathbf{A}(+z_s) \langle \mathbf{P}^-(z_0; z_0) \rangle \mathbf{F}^-(z_0, +z_s), \quad (7)$$

$$\langle \mathbf{P}^-(z_0; -z_s) \rangle = \mathbf{P}^-(z_0; \pm z_s) - \mathbf{A}(-z_s) \langle \mathbf{P}^-(z_0; z_0) \rangle \mathbf{W}^+(z_0, -z_s), \quad (8)$$

where diagonal matrices \mathbf{A} make the subtraction adaptive and the underscore symbol indicates a nonlinear-filter result (Figures 2e,f).

The estimates obtained in this way are the input to the next iteration: they are substituted in equations (2) and (3) respectively. At each subsequent iteration the threshold is lowered until no further improvement is obtained any more. The results are *two* data sets corresponding to the real sources at $+z_s$ and the ghost sources at $-z_s$, respectively. From equations (2) and (3) it follows that knowledge about the reflectivity of the water surface, as well as about the speed of sound in the water layer

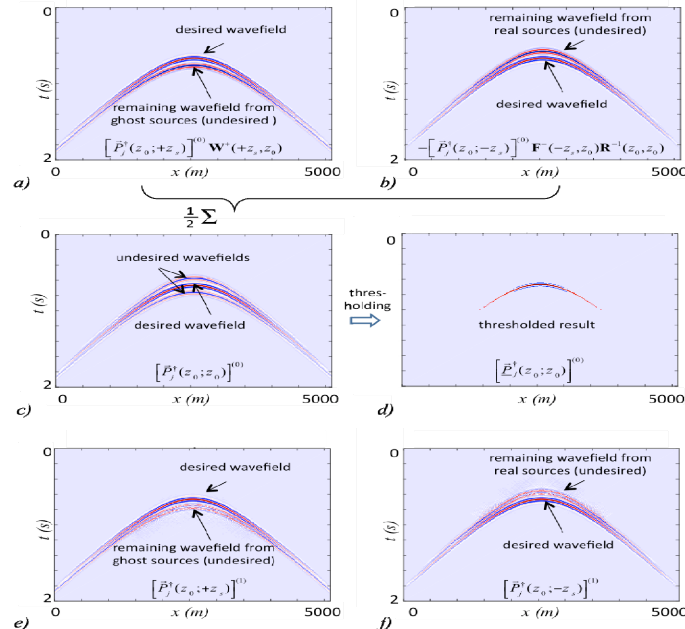


Figure 2 Single-reflector illustration for sources at 70 m (first iteration). The process starts by bringing the real and ghost sources to the surface (a,b). After averaging (c), the result is thresholded to suppress the undesired wavefields (d). Next, an estimate of the deblended result is obtained by wavefield extrapolation of the thresholded result to $\pm z_s$ (yielding the blending noise), followed by adaptive subtraction (yielding the desired wavefields) in (e,f).

between levels z_0 and $+z_s$ is key to our method: \mathbf{R} , \mathbf{W}^+ and \mathbf{F}^- are computed based on this information! Therefore, we propose to acquire temperature, salinity and sea-state information during acquisition, leading to accurate initial estimates of the ghost model: \mathbf{R} , \mathbf{W}^+ and \mathbf{F}^- . Further refinements should be estimated from the data and/or taken care of by the adaptive subtraction in equations (7,8).

The same echo-deblending concept can be used at the detector side as well. The theory is similar. We illustrate this by providing the detector-side equivalent of equation (1):

$$\mathbf{P}^-(\pm z_d; \mathbf{z}_0) = [\mathbf{F}^+(+z_d; \mathbf{z}_0) - \mathbf{W}^-(-z_d; \mathbf{z}_0)\mathbf{R}] \mathbf{P}^-(\mathbf{z}_0; \mathbf{z}_0) \quad (9)$$

where $z_d = z_d(x,y)$ represents the depth of the detectors. The fact that \mathbf{F} and \mathbf{W} are now applied at the left side of \mathbf{P} means that common source gathers are extrapolated. Figure 6a shows a simulated blended shot record (blending factor three) that has been recorded by a slanted cable, the detector depth $+z_d$ ranging from 10 m to 60 m for the lateral coordinate ranging from 0 m to 6000 m. The echo-deblended result is shown in Figure 6b. In Figures 6c,d the example has been repeated with -6 dB background noise. No special measures were taken to attenuate the noise. The output shows that the echo-deblending approach is robust for background noise. Finally, in Figure 7 a real-data example is shown. The data was acquired with a slanted cable. The depth varies from 5 m to 55 m, see Figure 7a. Figure 7b shows a shot record with the ghosts. The echo-deblending result is shown in Figure 7c. Note the excellent ghost removal, which is particularly clear in the area indicated by the white arrow.

Conclusions

A marine shot record represents a blended recording, with source(array)s at $+z_s$ and $-z_s$, the blending codes being +1 and $-\mathbf{R}$ respectively. Hence, deghosting can be considered as a deblending process. This alternative view leads to a full-wavefield algorithm that simultaneously takes the angle- and frequency-dependent properties of the near surface into account. The method is independent of the complexity of the subsurface. Results obtained from simulated and field data are according to theory: the deep ghost notches are removed and low-frequency information is enhanced. The method is robust for background noise, which is characteristic for deblending algorithms.

Acknowledgments

We acknowledge the members of the Delphi consortium for the stimulating discussions and their financial support.

References

- Soubaras, R. [2010] Deghosting by joint deconvolution of a migration and a mirror migration: *SEG Technical Program Expanded Abstracts*, **29** (1), 3406–3410.
- Wang, P., and Peng, C. [2012] Premigration deghosting for marine towed streamer data using a bootstrap approach: *SEG Technical Program Expanded Abstracts 2012*, **31**, 1–5.
- Amundsen, L., Zhou, H., Reitan, A., and Weglein, A.B. [2013] On seismic deghosting by spatial deconvolution: *Geophysics*, **78**, V267–V271.
- Beasley, C.J., Coates, R., Ji, Y., and Perdomo, J. [2013] Wave equation receiver deghosting: a provocative example: *SEG Technical Program Expanded Abstracts*, **32** (1), 4226–4230.
- Robertsson, J.O.A., Amundsen, L., and Pedersen, O. [2014] Deghosting of arbitrarily depth-varying marine hydrophone streamer data by time-space domain modelling, in *SEG Technical Program Expanded Abstracts 2014*, 4248–4252.
- Ferber, R., and Beasley, C.J. [2014] Simulating ultra-deep-tow marine seismic data for receiver deghosting: *76th Mtg., EAGE*.
- Mayhan, J.D., and Weglein, A.B. [2013], First application of greens theorem-derived source and receiver deghosting on deep-water gulf of mexico synthetic (seam) and field data: *Geophysics*, **78** (2), WA77–WA89.

Amundsen, L., and Zhou, H. [2013] Low-frequency seismic deghosting: *Geophysics*, **78**, WA15–WA20.

Berkhout, A.J., and Blacquière, G. [2014] Combining deblending with multi-level source deghosting: in *SEG Technical Program Expanded Abstracts 2014*, 41–45.

Berkhout, A.J., and Blacquière, G. [2013] Effect of noise in blending and deblending: *Geophysics*, **78** (5), A35–A38.

Orji, O.C., Sollner, W., and Gelius, L.J. [2013] Sea surface reflection coefficient estimation: in *SEG Technical Program Expanded Abstracts 2013*, 51–55.

Leroy, C.C., Robinson, S.P., and Goldsmith, M.J. [2008] A new equation for the accurate calculation of sound speed in all oceans: *Journal of Acoustical Society of America*, **124** (5), 2774–2782.

Berkhout, A.J. [1982] Seismic migration, imaging of acoustic energy by wave field extrapolation, A. theoretical aspects: *Elsevier*.

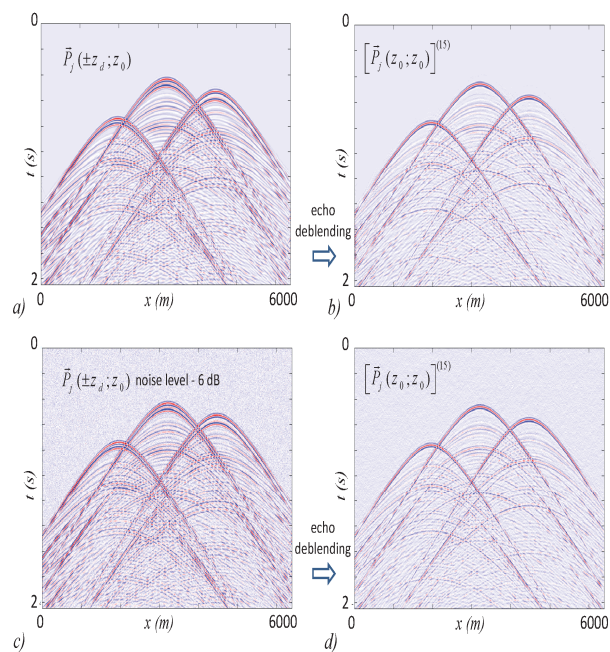


Figure 6 Echo-deblending at the detector side for man-made blending (blending fold 3). Input (a) and echo-deblended result (b) for a slanted streamer. In (c, d) idem with -6 dB background noise.

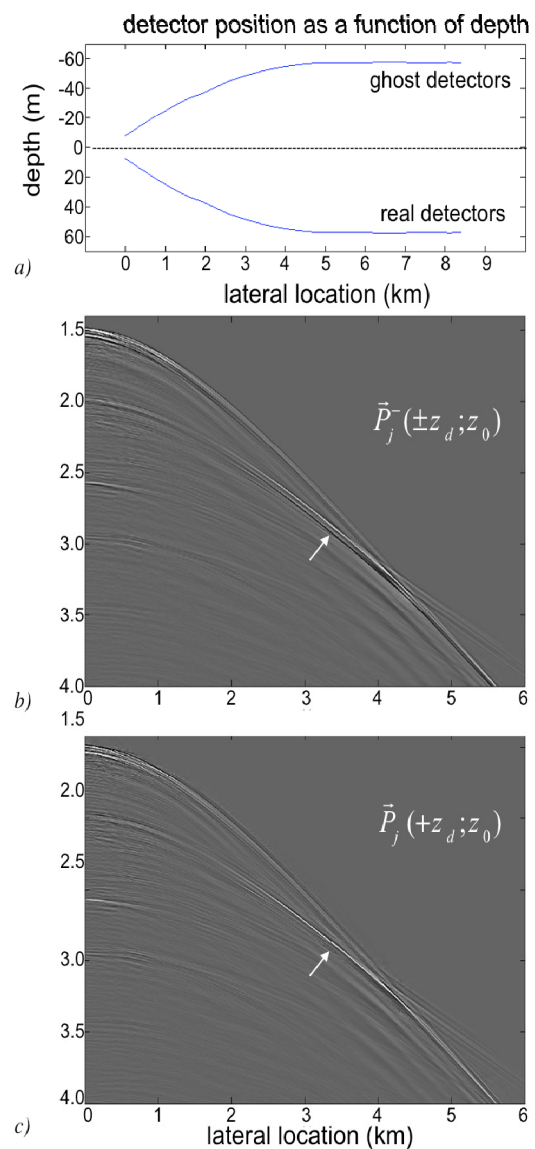


Figure 7 Echo-deblending at the detector side, where use was made of double-level streamer simulation; a) the real and ghost detector positions; b) input data; c) echo-deblending result